[Ir(N^N^N)(C^N)L]+: A New Family of Luminophores Combining Tunability and Enhanced Photostability

Danielle N. Chirdon,[†] Wesley J. Transue,[†] Husain N. Kagalwala,[†] Aman Kaur,[‡] Andrew B. Maurer,[†] Tomislav Pintauer,[‡] and Stefan Bernhard*,[†]

[†]Department of Chemistry, Carnegie Mellon University, Pittsburgh, Pennsylvania 15213, United States
[‡]Department of Chemistry and Biochemistry, Duquesne University, Pittsburgh, Pennsylvania 15282, United States

S Supporting Information

ABSTRACT: The relatively unexplored luminophore architecture [Ir(N^N^N)(C^N)L]+ (N^N^N = tridentate polypyridyl ligand, C^N = 2-phenylpyridine derivative, and L = monodentate anionic ligand) offers the stability of tridentate polypyridyl coordination along with the tunability of three independently variable ligands. Here, a new family of these luminophores has been prepared based on the previously reported compound [Ir(tpy)(ppy)Cl]+ (tpy = 2,2′:6′,2″-terpyridine and ppy = 2-phenylpyridine). Complexes are

obtained as single stereoisomers, and ligand geometry is unambiguously assigned via X-ray crystallography. Electrochemical analysis of the materials reveals facile HOMO modulation through ppy functionalization and alteration of the monodentate ligand's field strength. Emission reflects similar modulation shifting from orange to greenish-blue upon replacement of chloride with cyanide. Many of the new compounds exhibit impressive room temperature phosphorescence with lifetimes near 3 μs and quantum yields reaching 28.6%. Application of the new luminophores as photosensitizers for photocatalytic hydrogen generation reveals that their photostability in coordinating solvent is enhanced as compared to popular [Ir(ppy)2(bpy)]+ (bpy = 2,2′-bipyridine) photosensitizers. Yet, the binding of their monodentate ligand emerges as a source of instability during the redox processes of cyclic voltammetry and mass spectrometry. DFT modeling of electronic structure is provided for all compounds to elucidate experimental properties.
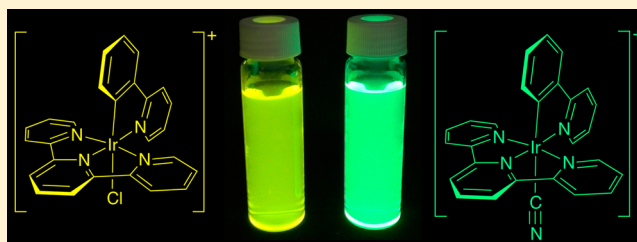
INTRODUCTION

Luminescent metal complexes continue to be important synthetic targets with applications ranging from catalysis and optoelectronics to biological imaging and gas sensing. Phosphorescent complexes are of particular interest due to their long-lived excited states and favorable spin statistics in organic light emitting devices (OLEDs). The archetype of phosphorescent compounds is [Ru(bpy)3]2+ (bpy = 2,2′-bipyridine), which has been studied with a plethora of derivatives in thousands of research publications;[1] however, ruthenium(II) complexes are almost exclusively orange emitting. Their emissive charge transfer triplet state (3MLCT) is deactivated via thermal population of a low-lying metal-centered triplet state (3MC).[2,3] Because the deactivating 3MC becomes more accessible with increases in the energy of the emissive state, efforts to blue-shift emission are largely thwarted by severe quenching. Significant interest in replacing ruthenium(II) luminophores has resulted, and popular candidates include square-planar d8 platinum(II) complexes[4] as well as tetrahedral d10 copper(I) compounds.[5] Period 6 d6 metals have also been explored with work focusing on metals which offer larger ligand field splitting than ruthenium(II) such as rhenium(I),[6] osmium(II),[7] iridium(III),[8] and platinum(IV).[9]

In iridium(III) complexes, large ligand field splitting renders thermal population of deactivating metal states unlikely, so the emissive triplet state is not limited by the energy ceiling imposed on ruthenium(II) materials. Instead, emission is completely tunable via ligand modifications. This versatility has expanded the possibilities for electron and energy transfer studies while installing iridium as a key material for phosphorescent light emitting diodes, solar fuel generation, light-driven organic chemistry, and a myriad of other applications.[10−14]

As with their ruthenium analogues, iridium(III) compounds often incorporate cyclometalating (C^N) and polypyridyl (N^N or N^N^N) ligands. Common structural motifs include [Ir(N^N)3]3+,[15] [Ir(N^N^N)2]3+,[16] [Ir(C^N)3],[17] and [Ir(C^N)2(N^N)]+. Among these, the latter heteroleptic structure is particularly popular with derivatives of [Ir(ppy)2(bpy)]+ (ppy = 2-phenylpyridine) emerging as leading small molecule photosensitizers for photocatalytic hydrogen evolution.[8a,b] Interest in these compounds as photosensitizers and as luminophores in general stems from their mixed metal to ligand and interligand charge transfer (MLCT/ILCT) excited state, which can be quenched oxidatively or reductively and can be readily tuned. The LUMO involved in excitation resides on the polypyridyl ligand while the HOMO is distributed over the
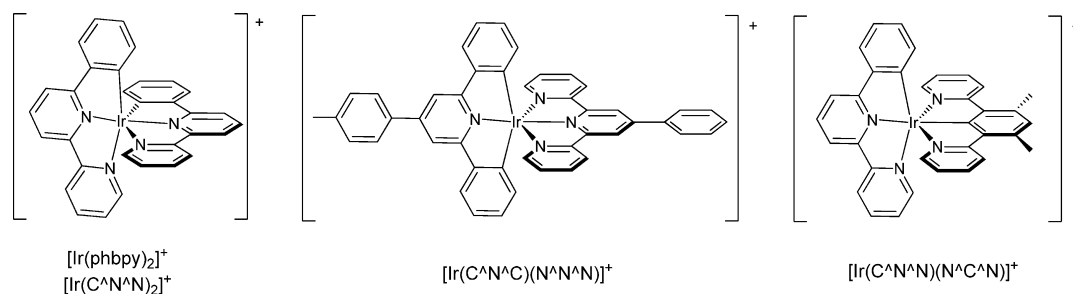
Figure 1. Common tridentate ligand arrangements which share the same basic coordination environment as the popular photosensitizer $[Ir(ppy)_2(bpy)]^+$.[18−20]

metal and the cyclometalating ligand. The spatial separation of the frontier orbitals enables independent control of their energies.

Unfortunately, the diimine ligand in $[Ir(C^\wedge N)_2(N^\wedge N)]^+$ luminophores is a source of photodegradation; it is susceptible to dissociation when charge transfer populates its π^* orbitals. To circumvent this weakness, the Bernhard lab has investigated $[Ir(phbpy)_2]^+$ (phbpy = 6′-phenyl-2,2′-bipyridine, Figure 1), which mimics the two carbon and four nitrogen coordination environment of $[Ir(ppy)_2(bpy)]^+$ while placing the LUMO on more stable tridentate ligands.[18] The new luminophore shows enhanced photostability, but its photophysics are ultimately altered in a way which diminishes its potential for device or catalytic applications. A variety of other tridentate ligand arrangements maintaining the same basic coordination environment have been reported such as $[Ir(C^\wedge N^\wedge C)(N^\wedge N^\wedge N)]^+$ and $[Ir(C^\wedge N^\wedge N)(N^\wedge C^\wedge N)]^+$ (Figure 1).[19,20] These structures can exhibit significant excited state lifetimes and spatial HOMO−LUMO separation similar to that in $[Ir(ppy)_2(bpy)]^+$. Yet, their synthesis is complicated by the multiple tridentate and bidentate binding modes available to their ligands.[21,22] Moreover, they tend to be less tunable than complexes with bidentate coordination since the extensive π systems of their tridentate ligands are more difficult to modify and more resistant to the impacts of simple, synthetically accessible changes.

The relatively unexplored structure $[Ir(N^\wedge N^\wedge N)(C^\wedge N)L]^+$ (L = anionic monodentate ligand) provides an interesting alternative for development of luminophores and photosensitizers. It has the potential to combine the stability of a $N^\wedge N^\wedge N$-centered LUMO with the tunability of a $C^\wedge N$ moiety and the added versatility of a third independently variable ligand. To the best of our knowledge, although a wide range of $[Ir(N^\wedge N^\wedge N)(N^\wedge N)Cl]^{2+}$ derivatives have been produced,[23] only three compounds of the form $[Ir(N^\wedge N^\wedge N)(C^\wedge N)L]^+$ have been previously reported.[21,24,25] Two of these are featured in Figure 2 while the third, $[Ir(tpy)(ppy)Cl]^+$ (tpy = 2,2′:6′,2″-terpyridine), is the starting point for this work. Sato et al. have recently introduced $[Ir(tpy)(ppy)Cl]^+$ as a photocatalyst for CO_2 reduction, but it has yet to be fully characterized.[25] Here, an entire series of compounds is based on that complex to methodically show the impact of individual ligand modifications on electrochemical and photophysical properties. Predictions of these properties and details of the electronic structure are obtained through DFT computations. Limitations of the computational models are also revealed. Lastly, testing of the new materials as photosensitizers in photocatalytic hydrogen evolution is included as proof of enhanced photostability.
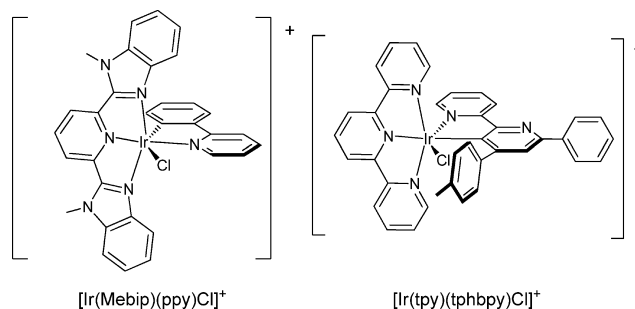
Figure 2. $[Ir(N^\wedge N^\wedge N)(C^\wedge N)L]^+$ type complexes previously reported by Obara et al. (left)[24] and Bexon et al. (right).[21]
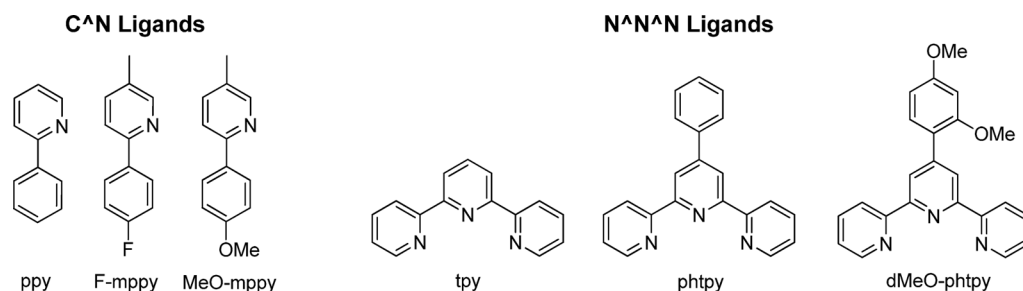
■ EXPERIMENTAL SECTION

General. 2-Phenylpyridine, 2,2′:6′,2″-terpyridine, IrCl$_3$·4H$_2$O, and all solvents were used as received from commercial sources. The F-mppy and MeO-mppy ligands (Figure 3) were synthesized according to the procedure of Lowry et al.[8c] 4′-Phenyl-2,2′:6′,2″-terpyridine was prepared as described by Wang and Hanan except the reaction mixture was stirred in the dark under argon, the reaction time was extended to 25 h, and product was recrystallized from an ethanol/water mix (98.5% EtOH v/v).[26] 4′-(2,4-Dimethoxyphenyl)-2,2′:6′,2″-terpyridine was prepared based on the procedure of Song et al.[27] with a slight modification: the reaction was stirred under argon for the given run time and then was pushed forward by adding excess aqueous ammonium acetate before refluxing in open air for 3.5 h.[28] ^{1}H and ^{13}C NMR spectra were recorded on Bruker Avance 300 and 500 MHz spectrometers. ESI-MS was performed with 50−60 μM acetonitrile and methanol solutions using a Thermo-Fisher LCQ instrument. Elemental analyses were conducted by Robertson Microlit Laboratories (Ledgewood, NJ).

Synthesis of [Ir(N^N^N)Cl$_3$]. Following the work of Collin et al.,[16b] the appropriate terpyridine ligand was combined with IrCl$_3$·4H$_2$O (1.1−1.2 equiv) and ethylene glycol (~14 mL/mmol ligand) in a two neck 25 mL round-bottom flask. This flask was placed under an argon atmosphere before stirring at 160 °C (**1a**) or 150 °C (**1b, 1c**) in the dark for 10 (**1b, 1c**) to 12 (**1a**) minutes. After cooling to room temperature, a dark red precipitate was collected via vacuum filtration and was washed with water, ethanol, and diethyl ether.

[Ir(tpy)Cl$_3$] (1a). Yield: 55%. ^{1}H NMR (300 MHz, DMSO-d_6): δ 9.22 (d, J = 5.5 Hz, 2H), 8.76 (d, J = 8.2 Hz, 2H), 8.72 (d, J = 7.8 Hz, 2H), 8.27 (t, J = 7.9 Hz, 2H), 8.23 (t, J = 8.1 Hz, 1H), 7.97 (dd, J = 7.5, 5.6 Hz, 2H). ^{13}C NMR (126 MHz, DMSO-d_6): δ 159.0, 157.2, 153.0, 140.4, 139.7, 128.3, 125.0, 123.5.

[Ir(phtpy)Cl$_3$] (1b). Yield: 59%. ^{1}H NMR (300 MHz, DMSO-d_6): δ 9.23 (dd, J = 5.6, 1.1 Hz, 2H), 9.11 (s, 2H), 8.92 (d, J = 7.9 Hz, 2H), 8.31 (td, J = 7.9, 1.5 Hz, 2H), 8.25−8.18 (m, 2H), 7.98 (ddd, J = 7.7, 5.5, 1.3 Hz, 2H), 7.75−7.67 (m, 2H), 7.65−7.59 (m, 1H). ^{13}C NMR (126 MHz, DMSO-d_6): δ 159.2, 157.3, 153.0, 151.1, 140.2, 135.2, 130.9, 129.2, 128.4, 128.3, 125.3, 121.1.

[Ir(dMeO-phtpy)Cl$_3$] (1c). Yield: 65%. ^{1}H NMR (300 MHz, DMSO-d_6): δ 9.22 (dd, J = 5.6, 1.1 Hz, 2H), 8.86 (s, 2H), 8.77 (d,

C^N Ligands

N^N^N Ligands

ppy   F-mppy   MeO-mppy   tpy   phtpy   dMeO-phtpy

Figure 3. Cyclometalating and polypyridyl ligands utilized in the new family of $[Ir(N^N^N)(C^N)L]^+$ luminophores.

J = 7.9 Hz, 2H), 8.26 (td, J = 7.9, 1.5 Hz, 2H), 7.96 (ddd, J = 7.8, 5.5, 1.3 Hz, 2H), 7.72 (d, J = 8.5 Hz, 1H), 6.87−6.79 (m, 2H), 3.94 (s, 3H), 3.91 (s, 3H). ^{13}C NMR (126 MHz, DMSO-d_6): δ 162.7, 159.3, 158.1, 156.5, 153.0, 149.5, 140.2, 132.3, 128.2, 125.0, 123.3, 117.5, 106.1, 98.8, 56.0, 55.7.

Synthesis of [Ir(tpy)(C^N)Cl](PF$_6$) Compounds. $[Ir(tpy)Cl_3]$ (80 mg, 0.15 mmol) and the appropriate cyclometalating ligand (c. 0.70 mmol) were placed under an argon atmosphere in a test tube before ethylene glycol (5 mL) was injected. The resulting mixture stirred overnight at 180 °C in darkness. After cooling in the dark, the reaction mixture was added to water (20 mL) and a yellow precipitate was seen. This solid could not be readily isolated by vacuum filtration, so the aqueous suspension was washed with chloroform (5 × 25 mL), and the subsequent emulsion was dissipated via vacuum filtration. Excess NH$_4$PF$_6$ (100 mg) was then added to the cloudy aqueous layer, and the mixture was stirred at room temperature for 1 h. Yellow precipitate was isolated by vacuum filtration and washed with water and diethyl ether.

[Ir(tpy)(ppy)Cl](PF$_6$) (2a). Yield: 61%. ^{1}H NMR (300 MHz, acetone-d_6): δ 10.11 (ddd, J = 5.9, 1.6, 0.8 Hz, 1H), 8.89 (d, J = 8.2 Hz, 2H), 8.73 (ddd, J = 8.1, 1.4, 0.8 Hz, 2H), 8.57 (dd, J = 8.5, 7.8 Hz, 1H), 8.47 (dt, J = 8.3, 1.1 Hz, 1H), 8.31 (ddd, J = 8.2, 7.5, 1.6 Hz, 1H), 8.23 (td, J = 7.9, 1.5 Hz, 2H), 7.93 (dd, J = 7.8, 1.4 Hz, 1H), 7.89 (ddd, J = 5.7, 1.6, 0.8 Hz, 2H), 7.80 (ddd, J = 7.4, 5.8, 1.4 Hz, 1H), 7.60 (ddd, J = 7.8, 5.6, 1.4 Hz, 2H), 6.96 (td, J = 7.6, 1.2 Hz, 1H), 6.78 (td, J = 7.5, 1.4 Hz, 1H), 6.14 (dd, J = 7.5, 1.1 Hz, 1H). ^{13}C NMR (126 MHz, acetone-d_6): δ 166.5, 158.3, 155.8, 151.9, 150.9, 144.0, 142.0, 140.2, 140.1, 130.6, 130.5, 128.9, 125.6, 125.1, 124.2, 124.1, 124.0, 120.5. MS (m/z; ESI, MeOH): 579.5 (100%, M − PF$_6$ − Cl), 615.1 (28%, M − PF$_6$). Elem. Anal. Calcd for $[IrC_{26}H_{19}N_4Cl]PF_6$·1/2(C$_4H_{10}$O): C, 42.19; H, 3.03; N, 7.03. Found: C, 41.97; H, 3.02; N, 6.89.

[Ir(tpy)(F-mppy)Cl](PF$_6$) (2b). Yield: 57%. ^{1}H NMR (300 MHz, acetone-d_6): δ 9.92 (s, 1H), 8.92 (d, J = 8.2 Hz, 2H), 8.75 (ddd, J = 8.1, 1.4, 0.7 Hz, 2H), 8.61 (dd, J = 8.5, 7.8 Hz, 1H), 8.34 (d, J = 8.4 Hz, 1H), 8.27 (td, J = 7.9, 1.5 Hz, 2H), 8.16 (ddd, J = 8.4, 2.1, 0.8 Hz, 1H), 7.97 (dd, J = 8.6, 5.5 Hz, 1H), 7.91 (ddd, J = 5.7, 1.5, 0.7 Hz, 2H), 7.62 (ddd, J = 7.8, 5.6, 1.4 Hz, 2H), 6.73 (td, J = 8.8, 2.5 Hz, 1H), 5.83 (dd, J = 9.0, 2.5 Hz, 1H), 2.63 (s, 3H). ^{13}C NMR (126 MHz, acetone-d_6): δ 158.3, 155.8, 152.0, 150.5, 140.9, 140.3, 140.2, 134.3, 128.9, 126.6 (d, J = 9.2 Hz), 125.7, 124.3, 120.0, 116.8 (d, J = 18.9 Hz), 110.9 (d, J = 22.9 Hz), 17.6. MS (m/z; ESI, MeOH): 611.5 (100%, M − PF$_6$ − Cl), 647.1 (36%, M − PF$_6$). Elem. Anal. Calcd for $[IrC_{27}H_{20}N_4FCl]PF_6$: C, 40.94; H, 2.54; N, 7.07. Found: C, 40.87; H, 2.38; N, 6.93.

[Ir(tpy)(MeO-mppy)Cl](PF$_6$) (2c). Yield: 47%. ^{1}H NMR (300 MHz, acetone-d_6): δ 9.87 (s, 1H), 8.90 (d, J = 8.2 Hz, 2H), 8.73 (ddd, J = 8.1, 1.3, 0.7 Hz, 2H), 8.57 (dd, J = 8.5, 7.8 Hz, 1H), 8.24 (td, J = 8.0, 1.6 Hz, 3H), 8.08 (ddd, J = 8.5, 2.1, 0.8 Hz, 1H), 7.91 (ddd, J = 5.7, 1.5, 0.7 Hz, 2H), 7.84 (d, J = 8.6 Hz, 1H), 7.62 (ddd, J = 7.8, 5.6, 1.4 Hz, 2H), 6.56 (dd, J = 8.6, 2.5 Hz, 1H), 5.51 (d, J = 2.5 Hz, 1H), 3.50 (s, 3H), 2.59 (s, 3H). ^{13}C NMR (126 MHz, acetone-d_6): δ 163.8, 160.5, 158.3, 155.9, 151.9, 150.0, 143.4, 140.6, 140.1, 140.0, 136.6, 133.0, 128.8, 126.3, 125.6, 124.1, 119.2, 116.1, 108.5, 54.2, 17.6. MS (m/z; ESI, MeOH): 623.4 (100%, M − PF$_6$ − Cl), 659.2 (31%, M −

PF$_6$). Elem. Anal. Calcd for $[IrC_{28}H_{23}N_4OCl]PF_6$: C, 41.82; H, 2.88; N, 6.97. Found: C, 41.63; H, 2.73; N, 6.68.

Synthesis of [Ir(tpy)(C^N)(CN)](PF$_6$) Compounds. $[Ir(tpy)Cl_3]$ (80 mg, 0.15 mmol) and the appropriate cyclometalating ligand (c. 0.70 mmol) were placed under an argon atmosphere in a test tube, and ethylene glycol (5 mL) was injected. The reaction mixture was stirred overnight at 180 °C in darkness. After cooling to 90 °C in the dark, the reaction mix was injected with KCN (20 mg, 0.30 mmol) in minimal water (0.2 mL) and was left to stir at 90 °C for an additional 1−2 h. The mixture was then cooled to room temperature and poured into water (20 mL). The resulting suspension was washed with chloroform (5 × 25 mL) and vacuum filtered to break up the subsequent emulsion. NH$_4$PF$_6$ (∼100 mg) was added to the aqueous layer before it was stirred at room temperature for 1 h. Yellow precipitate was then isolated by vacuum filtration and washed with water and diethyl ether.

[Ir(tpy)(ppy)(CN)](PF$_6$) (3a). Yield: 45%. ^{1}H NMR (300 MHz, acetone-d_6): δ 10.02 (ddd, J = 5.8, 1.6, 0.8 Hz, 1H), 8.99 (d, J = 8.2 Hz, 2H), 8.81 (dq, J = 7.9, 0.7 Hz, 2H), 8.68 (t, J = 8.2 Hz, 1H), 8.50 (dt, J = 8.2, 1.0 Hz, 1H), 8.37 (ddd, J = 8.4, 7.6, 1.6 Hz, 1H), 8.30 (td, J = 7.9, 1.5 Hz, 2H), 8.07 (ddd, J = 5.7, 1.5, 0.7 Hz, 2H), 7.96 (dd, J = 7.9, 1.2 Hz, 1H), 7.83 (ddd, J = 7.4, 5.8, 1.4 Hz, 1H), 7.65 (ddd, J = 7.7, 5.6, 1.4 Hz, 2H), 7.00 (td, J = 7.6, 1.2 Hz, 1H), 6.83 (td, J = 7.4, 1.2 Hz, 1H), 5.98 (dd, J = 7.6, 1.2 Hz, 1H). ^{13}C NMR (126 MHz, acetone-d_6): δ 167.5, 157.9, 155.1, 154.9, 153.9, 152.1, 140.2, 140.0, 139.9, 130.5, 129.7, 129.0, 125.9, 125.2, 124.6, 121.1. MS (m/z; ESI, MeOH): 579.5 (100%, M − PF$_6$ − CN), 606.3 (60%, M − PF$_6$). Elem. Anal. Calcd for $[IrC_{27}H_{19}N_5]PF_6$·1/2(C$_2$H$_3$N): C, 43.61; H, 2.68; N, 9.99. Found: C, 43.84; H, 2.42; N, 10.00.

[Ir(tpy)(F-mppy)(CN)](PF$_6$) (3b). Yield: 44%. ^{1}H NMR (300 MHz, acetone-d_6): δ 9.83 (dt, J = 2.2, 0.8 Hz, 1H), 8.99 (d, J = 8.2 Hz, 2H), 8.81 (ddd, J = 8.2, 1.4, 0.7 Hz, 2H), 8.68 (dd, J = 8.5, 7.8 Hz, 1H), 8.38 − 8.24 (m, 3H), 8.19 (ddd, J = 8.4, 2.0, 0.8 Hz, 1H), 8.07 (ddd, J = 5.6, 1.5, 0.7 Hz, 2H), 8.03 − 7.93 (m, 1H), 7.65 (ddd, J = 7.8, 5.6, 1.4 Hz, 2H), 6.73 (td, J = 8.9, 2.6 Hz, 1H), 5.63 (dd, J = 8.6, 2.6 Hz, 1H), 2.65 (s, 3H). ^{13}C NMR (126 MHz, acetone-d_6): δ 157.9, 154.9, 153.5, 152.2, 140.9, 140.2, 140.1, 135.3, 129.1, 126.9 (d, J = 8.7 Hz), 126.0, 124.9, 120.6, 116.0 (d, J = 17.6 Hz), 111.4 (d, J = 22.8 Hz), 17.6. MS (m/z; ESI, MeOH): 611.5 (100%, M − PF$_6$ − CN), 638.2 (86%, M − PF$_6$). Elem. Anal. Calcd for $[IrC_{28}H_{20}N_5F]PF_6$: C, 42.97; H, 2.58; N, 8.95. Found: C, 42.72; H, 2.29; N, 8.69.

Synthesis of [Ir(phtpy)(ppy)Cl](PF$_6$) (2d). $[Ir(phtpy)Cl_3]$ (72 mg, 0.119 mmol), ppy (71.25 μL, 0.499 mmol), and ethylene glycol (3.7 mL) were combined in a test tube. The tube was placed under argon atmosphere and stirred at 174 °C for 17 h in darkness. Water (8.0 mL) was added to the cooled reaction mixture, and the resulting aqueous solution was extracted with DCM (4 × 6.5 mL) as well as ether (2 × 8.0 mL). The aqueous phase was gently heated to remove residual ether and was filtered. NH$_4$PF$_6$ (80 mg) was added, and the resulting orange precipitate was collected via vacuum filtration. Collected solid was washed with water and recrystallized through vapor diffusion of pentane into acetone. Yield 50%. ^{1}H NMR (300 MHz, acetone-d_6): δ 10.13 (dq, J = 5.9, 0.7 Hz, 1H), 9.23 (s, 2H), 8.94 (dq, J = 8.1, 0.7 Hz, 2H), 8.48 (d, J = 8.0 Hz, 1H), 8.33 (m, 1H), 8.30−8.22 (m, 4H), 7.97- 7.89 (m, 3H), 7.82 (dd, J = 7.5, 1.4 Hz, 1H), 7.78−7.66 (m, 3H), 7.61 (dd, J = 8.0, 1.3 Hz, 2H), 6.96 (td, J = 7.5, 1.0 Hz, 1H), 6.78 (td, J = 7.5, 1.4 Hz, 1H), 6.27 (dd, J = 7.7, 0.9 Hz,

1H). ^{13}C NMR (126 MHz, acetone-d_6): δ 159.4, 156.8, 153.3, 152.9, 151.9, 141.1, 140.9, 132.0, 131.6, 131.4, 130.4, 129.8, 129.1, 126.7, 126.0, 125.1, 124.9, 122.7, 121.5. MS (m/z; ESI, MeOH): 655.5 (100%, M − PF_6 − Cl), 691.2 (97%, M − PF_6). Elem. Anal. Calcd for $[IrC_{32}H_{23}N_4Cl]PF_6$: C, 45.96; H, 2.77; N, 6.70. Found: C, 45.78; H, 2.58; N, 6.50.

Synthesis of [Ir(phtpy)(ppy)Cl](PF$_6$) Derivatives (2e, 2f, 2g). The appropriate $[Ir(N^\wedge N^\wedge N)Cl_3]$ compound (0.122 mmol) was combined with cyclometalating ligand (3−4 equiv) and ethylene glycol (∼3.8 mL) in a test tube. The tube was purged with argon and was stirred while heating at 179 °C for 18.2 h in the dark. After cooling for several hours, the reaction mixture was diluted with ethanol (∼3 mL) and then water (∼6 mL). The resulting solution was extracted with ether (4 × 10.5 mL), giving an aqueous layer, which was filtered and heated to remove residual ether. NH_4PF_6 (95 mg) was added, and precipitate was collected via vacuum filtration. Solid was washed with ether and water before it was recrystallized through vapor diffusion recrystallization (ether/acetonitrile for **2f**, pentane/acetone for **2e** and **2g**).

[Ir(phtpy)(F-mppy)Cl](PF$_6$) (2e). Yield: 63%. ^1H NMR (300 MHz, acetone-d_6): δ 9.94−9.91 (m, 1H), 9.22 (s, 2H), 8.95 (dq, J = 8.2, 0.7 Hz, 2H), 8.37−8.23 (m, 5H), 8.16 (dd, J = 8.4, 0.6 Hz, 1H), 7.97 (dd, J = 8.7, 5.6 Hz, 1H), 7.92 (dq, J = 5.7, 0.7 Hz, 2H), 7.77−7.67 (m, 3H), 7.62 (dd, J = 7.9, 1.4 Hz, 2H), 6.72 (td, J = 8.9, 2.6 Hz, 1H), 5.96 (dd, J = 8.9, 2.6 Hz, 1H), 2.62 (s, 3H). ^{13}C NMR (126 MHz, acetone-d_6): δ 159.5, 156.8, 152.9, 151.5, 141.9, 141.1, 132.0, 130.4, 129.8, 129.1, 127.6, 127.5, 126.8, 123.0, 120.9, 117.9, 117.8, 111.9, 111.7, 49.8 (solvent impurity), 18.6. MS (m/z; ESI, MeOH): 687.4 (69%, M − PF_6 − Cl), 723.1 (100%, M − PF_6). Elem. Anal. Calcd for $[IrC_{33}H_{24}N_4FCl]PF_6$: C, 45.65; H, 2.79; N, 6.45. Found: C, 45.58; H, 2.49; N, 6.29.

[Ir(phtpy)(MeO-mppy)Cl](PF$_6$) (2f). Yield: 56%. ^1H NMR (300 MHz, acetone-d_6): 9.90−9.86 (m, 1H), 9.21 (s, 2H), 8.94 (dq, J = 8.2, 0.5 Hz, 2H), 8.31−8.20 (m, 5H), 8.08 (ddd, J = 8.5, 2.1, 0.5 Hz, 1H), 7.92 (dq, J = 5.6, 0.7 Hz, 2H), 7.84 (d, J = 8.7 Hz, 1H), 7.77−7.67 (m, 3H), 7.62 (dd, J = 7.8, 1.5 Hz, 2H), 6.56 (dd, J = 8.5, 2.5 Hz, 1H), 5.63 (d, J = 2.5 Hz, 1H), 3.50 (s, 3H), 2.59 (s, 3H). ^{13}C NMR (126 MHz, acetone-d_6): δ 159.4, 156.9, 152.9, 151.0, 141.5, 140.9, 131.9, 130.4, 129.7, 129.1, 127.2, 126.7, 122.8, 120.1, 117.3, 109.2, 55.1, 18.5. MS (m/z; ESI, MeOH): 699.5 (31%, M − PF_6 − Cl), 735.1 (100%, M − PF_6). Elem. Anal. Calcd for $[IrC_{34}H_{27}N_4OCl]PF_6$: C, 46.39; H, 3.09; N, 6.36. Found: C, 46.17; H, 3.10; N, 6.38.

[Ir(dMeO-phtpy)(F-mppy)Cl](PF$_6$) (2g). Yield: 75%. ^1H NMR (300 MHz, acetone-d_6): 9.95−9.91 (m, 1H), 9.04 (s, 2H), 8.80 (dq, J = 8.2, 0.5 Hz, 2H), 8.32 (d, J = 8.2 Hz, 1H), 8.24 (td, J = 7.9, 1.5 Hz, 2H), 8.15 (ddd, J = 8.4, 2.1, 0.5 Hz, 1H), 7.96 (dd, J = 8.5, 5.5 Hz, 1H), 7.90−7.85 (m, 3H), 7.59 (ddd, J = 7.9, 5.6, 1.4 Hz, 2H), 6.91−6.82 (m, 2H), 6.72 (td, J = 8.9, 2.5 Hz, 1H), 5.92 (dd, J = 9.0, 2.5 Hz, 1H), 4.06 (s, 3H), 3.97 (s, 3H), 2.62 (s, 3H). ^{13}C NMR (126 MHz, acetone-d_6): δ 155.8, 152.9, 151.5, 141.8, 141.1, 133.2, 129.6, 126.5, 124.9, 120.9, 107.2, 99.7, 56.5, 56.2, 18.6. MS (m/z; ESI, MeOH): 747.4 (43%, M − PF_6 − Cl), 783.2 (100%, M − PF_6). Elem. Anal. Calcd for $[IrC_{35}H_{28}N_4O_2FCl]PF_6$: C, 45.29; H, 3.04; N, 6.04. Found: C, 45.00; H, 2.82; N, 5.88.

X-ray Crystallography. Single crystals of **2c** were grown for X-ray structure determination via slow diffusion of pentane into acetone. Resulting crystals contained one molecule of acetonitrile and ethylene glycol along with disordered unspecified electron density located in the lattice. This was removed by the SQUEEZE/PLATON technique,[29] and the estimated volume of the solvent accessible void per unit cell is 240 Å^3, indicating unrefined, disordered solvent molecules. The X-ray intensity data was collected at 150 K using graphite-monochromated Mo Kα radiation (λ = 0.71073 Å) on a Bruker Smart Apex II CCD diffractometer. Data reduction included absorption corrections by the multiscan method using SADABS.[30] Crystal data and detailed experimental conditions are given in the Supporting Information (Tables S1−S5). Structures were solved by direct methods and refined by full-matrix least-squares using the SHELXTL 6.1 bundled software package.[31] The H atoms were positioned geometrically (aromatic C−H = 0.93 Å, methylene C−H = 0.97 Å, and methyl C−H = 0.96 Å)
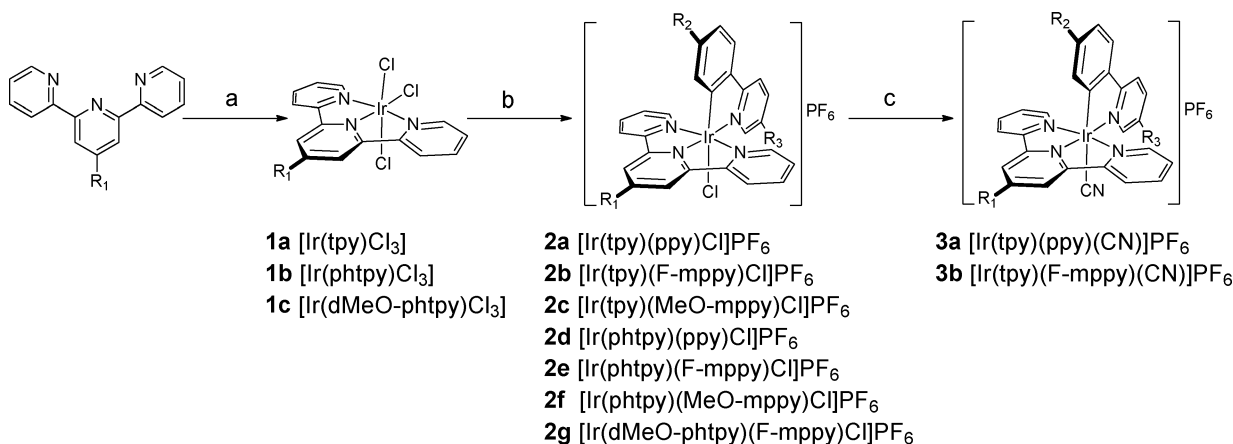
and treated as riding atoms during subsequent refinement, with $U_{iso}(H)$ = 1.2$U_{eq}(C)$ or 1.5U_{eq} (methyl C). The methyl groups were allowed to rotate about their local 3-fold axes. Crystal Maker 8.2 was used to generate molecular graphics.

Electrochemistry. Cyclic voltammograms were collected using a CH-Instruments Electrochemical Analyzer 600C potentiostat with a three electrode system consisting of a 1 mm^2 platinum disk working electrode, a coiled platinum counter electrode, and a silver wire pseudoreference.[32] Potential scans were performed under an argon purge in acetonitrile solutions containing 0.10 M tetrabutylammonium hexafluorophosphate as supporting electrolyte and 0.5−0.8 mM analyte. An internal ferrocene standard was added to each solution, and potentials were referenced to SCE by setting the ferrocene oxidation to 0.40 V.[33] Unless otherwise noted, positive scan polarity and a scan rate of 0.10 V/s were employed.

Computational Methodology. All DFT calculations were carried out with the Gaussian 03 suite.[34] Ground-state and excited-state geometries (both singlet and triplet) for all complexes were evaluated computationally using Becke's three-parameter exchange functional (B3)[35] in conjunction with the Lee, Yang, and Parr (LYP)[36,37] nonlocal functional using the default thresholds for gradient convergence. The LANL2DZ basis set was employed for all calculations.[38] The geometry optimization for complexes **2a** and **3a** was performed with a C_s symmetry restriction, but the same minimum energy and optimal coordinates were found without any constraints. To model the complexes immediately after radiative relaxation, the energy of a singlet electron configuration in the triplet geometry was calculated. For each complex, time-dependent DFT (TD-DFT) calculations were performed at the optimized ground-state geometry, calculating the energy and oscillator strength for each of the 70 lowest singlet excitations. Prediction of UV−vis absorption spectra was accomplished using GaussSum 2.0.[39] Electronic transitions were expanded as Gaussian curves with a full-width at half-maximum (fwhm) for each peak set at 4000 cm^{-1}.

Photophysical Characterization. Photophysical measurements were conducted at room temperature on 10 μM acetonitrile solutions which were purged with argon for 5 min in capped quartz cuvettes. UV−vis absorption spectra were obtained with a Shimadzu UV-1800 spectrophotometer. Photoluminescence was measured using a Fluorolog-3 spectrophotometer equipped with dual monochromators and a photomultiplier tube (PMT) at right angle geometry. All compounds were excited at 380 nm. In order to calculate excited state lifetimes, samples were pulsed at 337 nm with a Stanford Research Systems NL 100 N$_2$ laser as emission decay was monitored with an oscilloscope and converted into a linear regression via a Labview interface. Quantum yields were determined using a 10 μM $[Ru(bpy)_3]^{2+}$ reference and the expression $\phi_s = \phi_{ref}(I_s/I_{ref})(A_{ref}/A_s)(\eta_s/\eta_{ref})$[40] where ϕ_s is the sample's quantum yield, ϕ_{ref} is the reference's established quantum yield (6.2%),[41] I_s and I_{ref} represent maximum emission intensities for the sample and reference, A_s and A_{ref} are sample and reference absorbances at the excitation wavelength, and η_{ref} and η_s represent the refractive indices of the solvents used in reference and sample absorbance measurements. Emission intensities were corrected for the detector's response over the spectral range. Stern−Volmer analysis was performed by measuring emission from solutions under atmospheres containing 10%, 30.7%, or 100% O$_2$ at ambient pressure. Slopes of generated Stern−Volmer plots gave pressure-based Stern−Volmer constants (K_{svP}), which were converted to quenching constants k_q based on the expressions $K_{svP} = K_{sv}K_h$ and $K_{sv} = k_q\tau_0$ where K_{sv} is the concentration-based Stern−Volmer constant, K_h is the Henry's Law constant for O$_2$ solubility in acetonitrile (8.92 × 10^{-6} M mbar^{-1}),[42] and τ_0 is the excited state lifetime under argon.[43]

Photocatalytic Hydrogen Generation. Photocatalytic hydrogen generation was carried out following a fixed protocol described by Cline et al.[13d] Solutions containing 0.075 mM photosensitizer (PS) and 300 nmol of K$_2$PtCl$_4$ were made in 40 mL screw top vials (VWR) with 10 mL of solvent composed of 8 mL of acetonitrile (ACN), 1 mL of water, and 1 mL of triethylamine (TEA). Control vials were also prepared without either the PS, the catalyst, or TEA. All vials were

Scheme 1. Synthetic Pathway and Labels for Ir(III) Complexes[a]

1a [Ir(tpy)Cl₃]
1b [Ir(phtpy)Cl₃]
1c [Ir(dMeO-phtpy)Cl₃]

2a [Ir(tpy)(ppy)Cl]PF₆
2b [Ir(tpy)(F-mppy)Cl]PF₆
2c [Ir(tpy)(MeO-mppy)Cl]PF₆
2d [Ir(phtpy)(ppy)Cl]PF₆
2e [Ir(phtpy)(F-mppy)Cl]PF₆
2f [Ir(phtpy)(MeO-mppy)Cl]PF₆
2g [Ir(dMeO-phtpy)(F-mppy)Cl]PF₆

3a [Ir(tpy)(ppy)(CN)]PF₆
3b [Ir(tpy)(F-mppy)(CN)]PF₆

[a]Reaction conditions: (a) IrCl₃·4H₂O, ethylene glycol, argon atmosphere, 150−160 °C, 10−12 min. (b) C^N ligand, ethylene glycol, argon atmosphere, 174−180 °C, overnight. (c) KCN (aq), ethylene glycol, argon atmosphere, 90 °C, 1−2 h.

placed in a 16 well, water-cooled photoreactor mounted on an orbital shaker and equipped with pressure transducers as well as bottom LED illumination (Luxeon V Dental Blue LEDs, LXHL-LRD5 with collimating optics Fraen FHS-HNB1-LL01-H). With the transducers screwed onto the vials, the vials were vacuum degassed and filled with Ar gas 7 times before the vial headspace was allowed to come to atmospheric pressure. The orbital shaker was then started (100 rpm) and samples were illuminated at room temperature. H₂ generation was monitored by conversion of pressure transducer readings into pressure traces using a LabView PC interface. Illumination was continued till no further increase in the traces was observed. Analysis of the reaction headspace of each vial was performed using a residual gas analyzer (RGA), precalibrated using 10% and 30% H₂/Ar mixtures.

■ RESULTS AND DISCUSSION

Synthesis and Design. The family of compounds prepared here (Scheme 1, Figure 3) can be divided into three subsets based on their tridentate and monodentate ligands: **2a−2c** (N^N^N = 2,2′:6′,2″-terpyridine and L = Cl⁻), **2d−2f** (N^N^N = 4′-phenyl-2,2′:6′,2″-terpyridine derivative and L = Cl⁻), and **3a** and **3b** (N^N^N = 2,2′:6′,2″-terpyridine and L = CN⁻). Within each subset, the phenylpyridine was functionalized in order to alter its electron density and determine whether it is a key site for HOMO modulation as in other cyclometalated iridium(III) materials.[44−47] Compound **2g** was more specifically designed with an electron poor cyclometalating ligand across from an electron rich tridentate ligand to explore the possibility of creating a "push−pull" force on electrons.

All chloro complexes (**2a−2g**) were readily synthesized in two steps: Tridentate ligand was added to IrCl₃·4H₂O to give [Ir(N^N^N)Cl₃], which was then cyclometalated with excess ppy or ppy derivative. Exclusion of light as well as control of run time and temperature were critical to the purity of products in both steps. Cyano complexes were formed from corresponding chloro materials through cyanide−chloride exchange directly after the cyclometalation reaction in the same pot. Although isomer formation previously complicated preparation of the similar complex [Ir(Mebip)(ppy)Cl]⁺ (Figure 2),[24] one stereoisomer was readily obtained here from all cyclometalation and ligand exchange reactions.

Phenylterpyridine (phtpy) ligands were prepared using a modified Kröhnke pathway in which condensation of 2-acetylpyridine and a benzaldehyde is followed by ring closure.

Ligand synthesis was based on literature procedures carried out in open air,[26,27] but use of argon atmosphere during condensation was found to limit byproducts. Air, meanwhile, was required for ring closure in 4′-(2,4-dimethoxyphenyl)-2,2′:6′,2″-terpyridine (dMeO-phtpy).[28]

X-ray Crystallography. Crystallography was critical for unambiguously identifying the obtained stereoisomer of the complexes. Possible isomers position the ppy with its cyclometalating carbon either cis or trans to the monodentate ligand. The structure determined from a single crystal of **2c** (Figure 4) shows that MeO-mppy is coordinated with its
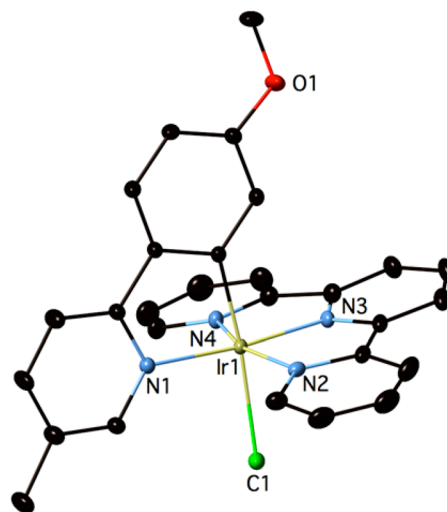

Figure 4. Crystal structure of **2c** shown with 30% thermal ellipsoids. Hydrogen atoms, the counterion (PF₆⁻), and solvent molecules are omitted for clarity.

cyclometalating carbon trans to the chloride ligand, an orientation seen previously in the isolated isomer of [Ir-(Mebip)(ppy)Cl]⁺ (Figure 2).[24] The strong trans influence of the cyclometalated carbon in **2c** causes the Ir−Cl bond to be significantly elongated (2.4457(6) Å) when compared to similar iridium complexes with noncyclometalating bidentate ligands: [Ir(tpy)(bpy)Cl]²⁺ (2.335 Å) or [Ir(tpy)(dmbpy)Cl]²⁺ (2.357 Å).[48,49] The bite angle (N1−Ir1−C1 = 80.69(9)°) and bond lengths (Ir1−C1 = 2.021(2) Å and Ir1−N1 = 2.068(2)
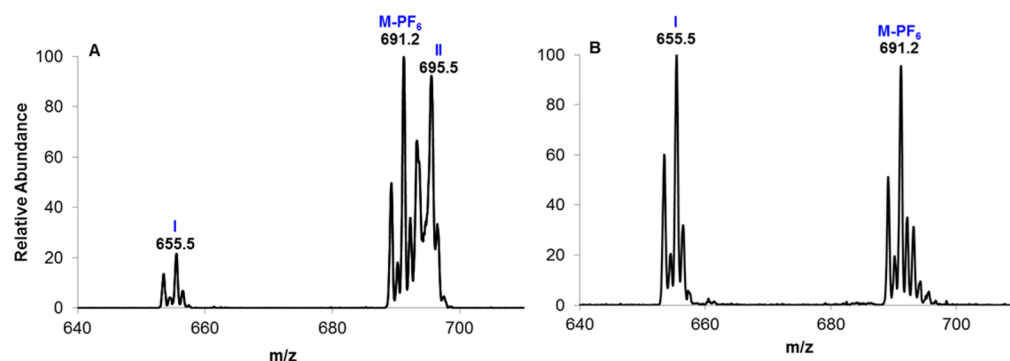
Figure 5. Electrospray ionization mass spectra collected for **2d** in (A) acetonitrile and (B) methanol. Peak m/z values are given with black labels while assignments are made in blue. Spectra were collected with 50−60 μM solutions.
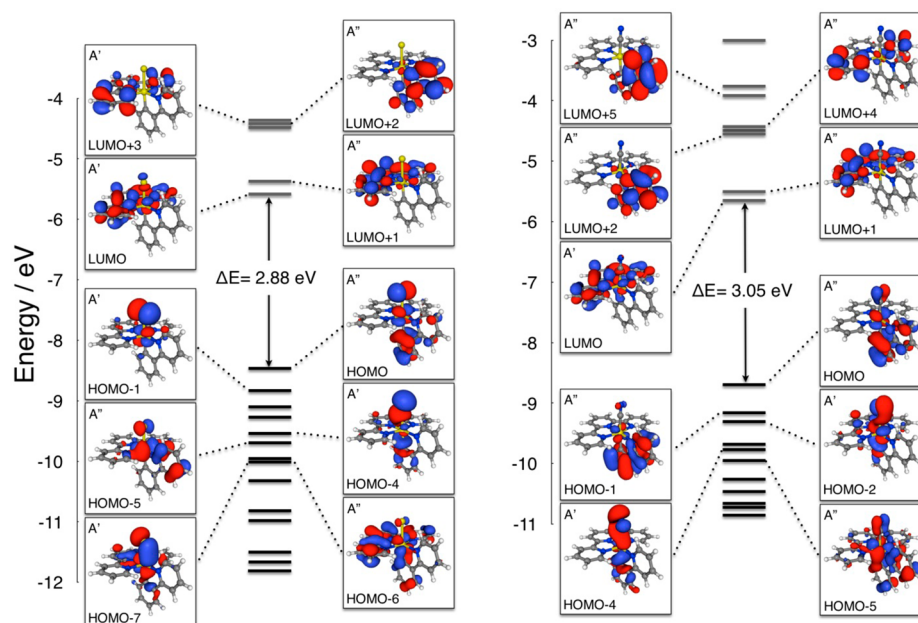
Figure 6. Frontier orbital diagram constructed for **2a** (left) and **3a** (right) from DFT calculations performed with Gaussian software[34] and displayed via Molekel.[52] C_s symmetry labels are provided for the orbitals.

Å) for MeO-mppy are very similar to the values reported for ppy in $[Ir(ppy)_3]$.[50] The iridium(III) center in **2c** adopts a distorted octahedral geometry due to constraints imposed by the planar tpy ligand. The tpy is coordinated to the iridium via all three of its nitrogen atoms in a meridional arrangement with relatively small bite angles (N2−Ir1−N3 = 80.38(9)° and N3−Ir1−N4 = 80.29(9)°). Lengths of Ir−N bonds involving tpy's two peripheral pyridine rings (Ir1−N2 = 2.040(2) Å and Ir1−N4 = 2.035(2) Å) are longer than the iridium bond with the central ring (Ir1−N3 = 1.944(2) Å) as observed previously in compounds of the type $[Ir(tpy)_2]^{3+}$ and $[Ir(tpy)(bpy)-Cl]^{2+}$.[16b,49,51] All bond lengths and angles are available in the Supporting Information (Tables S4 and S5).

Mass Spectrometry. The electrospray ionization mass spectrum collected for **2d** in acetonitrile is presented in Figure 5 as a representative example for **2a**−**3b**. It shows the expected M − PF$_6$ signal grouping (m/z = 691.2), but it also contains two other groupings labeled I (m/z = 655.5) and II (m/z = 695.5). Since NMR results show a single set of peaks, I and II must stem from compounds which are not intrinsic to the sample and instead form during electrospray ionization. Separation between I and the M − PF$_6$ grouping equals the

mass of the monodentate ligand suggesting that I represents the product of monodentate ligand dissociation, $[Ir(phtpy)-(ppy)]^{2+}$. Grouping II, meanwhile, is consistent with a complex in which an acetonitrile solvent molecule replaces the monodentate ligand. Its separation from the $[Ir(phtpy)-(ppy)]^{2+}$ grouping (I) matches acetonitrile's mass within resolution limits, and it is completely eliminated by replacement of acetonitrile with less coordinating methanol solvent. Furthermore, elimination of II markedly increases the abundance of I confirming I and II as competing forms of an electrospray ionization product. Mass spectra for all compounds mirror the three features of **2d** with variation limited to relative abundances.

Static DFT Calculations. The nuclear geometries and electronic structures of the complexes were investigated with DFT calculations using the B3LYP functional and the LANL2DZ basis set. DFT calculations of **2a**'s possible isomers estimate that the trans isomer observed for **2c** via crystallography is 8.6 kcal/mol more stable than its counterpart having ppy's cyclometalating carbon cis to the chloride. Frontier orbitals generated for **2a** and **3a** are compared in Figure 6. The LUMO in both complexes is exclusively located

on the terpyridine ligand and exhibits A′ symmetry. The A″ HOMO resembles that of the well-studied $[Ir(ppy)_2(bpy)]^+$ complexes showing large involvement of the ppy's phenyl ring and an iridium d orbital.[44,45,47] However, prominent contributions are also made by an antibonding interaction between the metal and the monodentate ligand.

Replacement of the chloride ligand with a stronger field cyanide capable of backbonding reduces the HOMO energy by 0.24 eV and subsequently broadens the HOMO−LUMO gap. Substitution of ppy adjusts calculated HOMO energies within a 0.433 eV range. Other tuning strategies, meanwhile, are predicted to have mixed results. Addition of an aryl moiety to terpyridine has little impact failing to extend the LUMO beyond terpyridine's three coordinating pyridyl rings except in **2g**. There, the LUMO is predicted to include dMeO-phtpy's methoxy substituents.

Electrochemistry. Rich electrochemistry was observed for the iridium compounds via cyclic voltammetry (Tables 1 and

Table 1. Electrochemical Properties of $[Ir(N^N^N)(C^N)Cl]PF_6$ Compounds

| compound	oxidation[a] E_{pa}/V	reduction[a]		
		I: $E_{1/2}$/V (ΔE/mV)	II:[d] E_{pc}/V	III: E_{red}/V (ΔE/mV)
2a	1.72, 2.09[c]	−1.09 (61)	−1.35	−1.98[e]
2b	1.78, 2.01	−1.07 (69)	−1.39	−1.92[e]
2c	1.45	−1.09 (73)	−1.41	−1.95(85)[f]
2d	1.71	−1.06 (78)	−1.39	−1.95[e]
2e	1.77, 2.08	−1.05 (71)	−1.37	−1.92[e]
2f	1.45	−1.07 (75)	−1.42	−1.95[e]
2g	1.63,[b] 1.71	−1.10 (64)	−1.40	−1.98[e]

[a]Potentials were measured in 0.10 M N(n-Bu)$_4$PF$_6$ (MeCN) solution with a three electrode system scanning at 0.10 V/s. Potentials are given in V vs SCE, and peak separation is given in mV. [b]Shoulder. [c]Resolution from solvent oxidation is poor. [d]Irreversible. No anodic reversal of II is resolved from the reverse of I. [e]Irreversible. A competing oxidative process supersedes reversal of reduction at 0.10 V/s and gives an anodic peak shifted relative to the reduction by +0.20 V. [f]Quasi-reversible. Reversal of reduction is observed despite a competing process.

Table 2. Electrochemical Properties of $[Ir(N^N^N)(C^N)CN]PF_6$ Compounds

compound	oxidation:[a] E_{pa}/V	reduction:[a] $E_{1/2}$/V (ΔE/ mV)
3a	1.90[b]	−1.10 (65), −1.68 (68)
3b	2.04[b]	−1.07 (71), −1.66 (75)

[a]Potentials are given in V vs SCE and were collected under the same experimental conditions used for **2a−2g**. [b]Resolution from the solvent oxidation is poor.

2). All materials show at least one irreversible oxidation while many of the chloro compounds (Figure 7a) also show a second oxidation near the solvent window's positive edge. In addition to oxidation, cyano compounds exhibit two reversible reductions (Figure 7b) and members of the chloro series show three reductions of varying reversibility: a first reversible reduction (I), a second irreversible process (II), and a third reduction which is typically irreversible (III) (Figure 7a). The electrochemical features of the chloro compounds are strikingly similar to those described previously for [Re(dmbpy)-
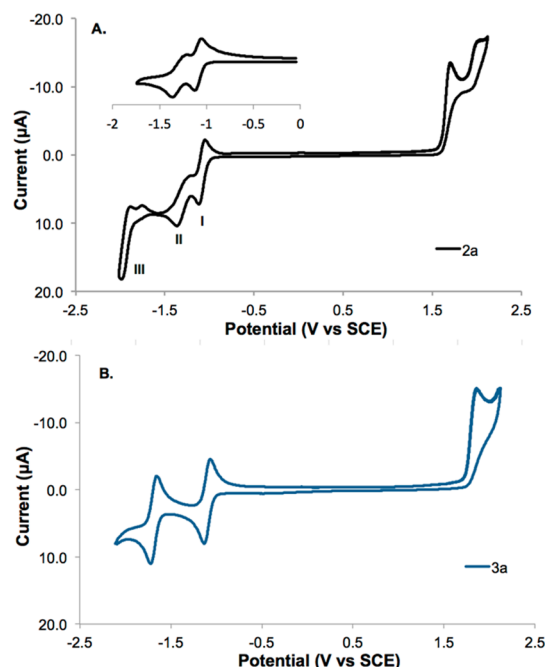
Figure 7. (A) Cyclic voltammogram of **2a** which exemplifies the main redox features of all compounds with a chloro monodentate ligand (**2a−2g**). Roman numeral labels denote three distinct types of reduction. The inset displays the first two reductions of **2a** scanned without observing process III. (B) Cyclic voltammogram of **3a** representing the redox behavior of the cyano complexes. All cyclic voltammograms were collected at 0.10 V/s using a three electrode system in 0.10 M N(n-Bu)$_4$PF$_6$ (MeCN) solutions. Potentials are referenced to SCE via an internal ferrocene standard (fc/fc$^+$ = 0.40 V).[33]

(CO)$_3$Cl].[53] Interestingly, both derivatives of the rhenium compound and the parent chloro compound (**2a**) have been used as catalysts for CO$_2$ reduction.[25,54] Their redox behavior may thus be related to catalytic performance and is given particular consideration for the compounds studied here.

For all compounds except **2g**, the first irreversible oxidation can be assigned as a metal-centered process with some participation of the ppy and monodentate ligands. First oxidation potentials reflect the effect of ppy modification on the HOMO and decrease expectedly as the ppy's electron density increases within the chloro or cyano series. Comparison between the two series reveals that the strong field cyano ligand causes the first oxidation to become significantly more difficult stabilizing the HOMO as predicted via DFT. Cyanide's strong field effect precludes observation of a second oxidation in **3a** and **3b**. However, such a process is seen in select chloro species where the ppy orbitals are sufficiently low in energy to avoid significant overlap with and stabilization of frontier metal orbitals. In specially designed **2g**, oxidation is different than in the other compounds consisting of two poorly resolved irreversible waves (Figure S3 in the Supporting Information). These likely represent typical metal-centered oxidation as well as oxidation of the electron rich dimethoxyphenyl moiety in dMeO-phtpy. The order of the processes cannot be unambiguously assigned, but calculations suggest that the ligand moiety is most easily oxidized (Supporting Information), which reflects the goal of **2g**'s design to push electrons away from that ligand.

First oxidations observed for the chloro and cyano complexes are significantly higher in potential and less reversible than those in more established bis-cyclometalated architectures [Ir(C^N)$_2$(bpy)]$^+$ ($E_{OX} \approx +1.25$ V vs SCE)[46] and [Ir-(C^N^C)(phtpy)]$^+$ ($E_{OX} \approx +1.09$ V vs SCE).[19b] The irreversibility may stem directly from dissociation of the monodentate ligand, which is shown to be possible for both chloride and cyanide via mass spectrometry. The possibility of cyanide dissociation is further supported by the previous report on [Re(dmbpy)(CO)$_3$Cl] ascribing the irreversibility of its metal oxidation to dissociation of an isoelectronic CO ligand as removal of metal electron density weakens backbonding.[53]

In all of the compounds, the first reduction occurs on the polypyridyl ligand as in both [Ir(ppy)$_2$(bpy)]$^+$ and [Ir-(C^N^C)(phtpy)]$^+$ structures.[19b,44,45] Accordingly, alterations to the ppy and monodentate ligand have little impact on the potential of the reduction. The potential also remains fairly constant despite additions of various phenyl groups to tpy. As predicted by computations, these groups are poor tuning tools and do not participate in the LUMO with tpy's three coordinating pyridines. The disconnect between the added phenyl groups and the coordinating pyridines arises from the lack of coplanarity between those moieties as evidenced by the crystal structure of [Ir(ttpy)(bpy)Cl]$^{2+}$ (ttpy = 4'-(4-tolyl)-2,2':6',2''-terpyridine).[51]

The second reduction in [Ir(ppy)$_2$(bpy)]$^+$ and [Ir(C^N^C)-(phtpy)]$^+$ is generally assigned to the cyclometalating ligand rather than to a second reduction of the polypyridyl group.[19b,44,45] A similar assignment seems logical for the new family of complexes, but their second reduction is surprisingly dependent on the monodentate ligand. Although the process is completely reversible in cyano complexes, it is consistently irreversible for chloro compounds regardless of whether the scan is reversed before or after the third reduction. Moreover, the process occurs more readily in the chloro series despite the greater electron deficiency of the iridium—cyanide bond which should facilitate reduction. Ligand dissociation is again suspected to play a key role. Cyanide is unlikely to dissociate and cause irreversibility during reduction due to strengthening of backbonding. Chloride, meanwhile, remains vulnerable as witnessed in [Re(dmbpy)(CO)$_3$Cl],[53] and its dissociation is forecast by DFT calculations showing metal—chloride bond elongation with increases in negative charge. Chloride's weak binding is further implicated in the irreversibility of the second reduction by the full reversibility of that process in the model compound [Ir(tpy)(ppy)(py)](PF$_6$)$_2$ where pyridine (py) binds more strongly than chloride (Figure S4 in the Supporting Information). Lastly, loss of chloride is consistent with the relative ease of the second reduction in the chloro series: Dissociation of chloride from a singly reduced complex lowers the overall negative charge alleviating repulsion of an incoming second electron.

Observation of a third reduction in chloro but not cyano complexes can also be explained by lowering of overall negative charge upon chloride loss. Yet, discussion of a similar process by Breikss et al. does not apply here, and the process cannot be unambiguously assigned at this time.[53] Reversal of the reduction is largely superseded by another process signified by an anodic peak shifted from the reduction by ~+0.20 V. An increase in reversibility is observed at high scan rates (1.5 V/s) and is the only significant difference when reductions of **2a** are measured in noncoordinating THF instead of acetonitrile. Thus, acetonitrile binding may give rise to the competing

process (Figure S5 in the Supporting Information). Spectroscopic evidence is needed to confirm coordination changes suspected to occur during redox processes.

Measured redox potentials have been used to calculate excited state oxidation and reduction potentials, which are critical for photosensitization (Table 3). The excited states of

Table 3. Calculated Excited State Redox Potentials[55]

compound	$E([M^*]^+/[M]^{2+})/V^{a,b}$	$E([M^*]^+/[M]^0)/V^{a,c}$
2a	−0.57	1.20
2b	−0.56	1.27
2c	−0.77	1.13
2d	−0.56	1.21
2e	−0.53	1.25
2f	−0.77	1.15
2g	−0.67	1.20
3a	−0.60	1.40
3b	−0.52	1.49
[Ir(ppy)$_2$(bpy)](PF$_6$)^d	−0.85	0.68

^{a}All potentials are given in V vs SCE. $^bE([M^*]^+/[M]^{2+}) = E_{OX} - E_{\lambda em}$. $^cE([M^*]^+/[M]^0) = E_{red} + E_{\lambda em}$. ^{d}From ref 46.

2a−**3b** are not as highly reducing as those of iridium photosensitizers for hydrogen evolution (see [Ir(ppy)$_2$(bpy)]-(PF$_6$) in Table 3).[44,46] Nevertheless, the excited state reduction potentials show that the excited chloro and cyano compounds are stronger oxidants than some successful iridium materials indicating a possibility for effective photosensitization via reductive quenching.[44,46]
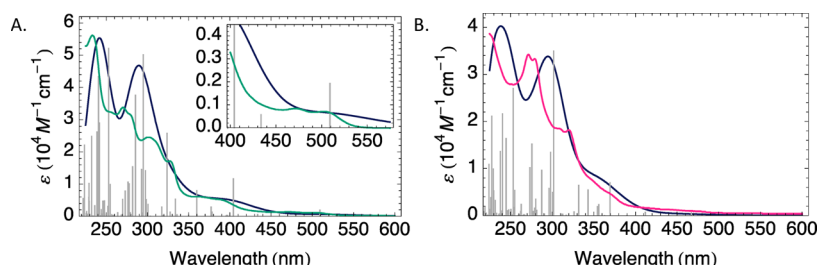
UV−Vis Absorption Spectroscopy. The absorption spectra of compounds **2a**, **2g**, and **3a** in acetonitrile are depicted in Figure 8 as representative examples for the new
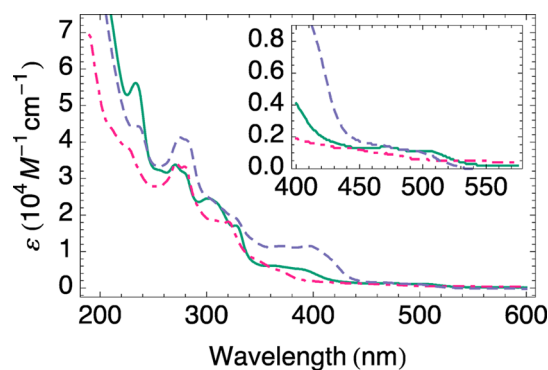
Figure 8. UV−vis absorption spectra for **2a** (green), **2g** (purple dashes), and **3a** (pink dashes). The portion of the spectrum from 400 to 580 nm is enlarged in the inset to show details of the weakest, low energy transition. All spectra were collected at room temperature for 10 μM acetonitrile solutions.

family of yellow to orange chromophores. The spectra lack any strong, defining features as observed for many iridium(III) complexes with cyclometalating and polypyridyl ligands including the similar [Ir(tpy)(tphbpy)Cl]$^+$ structure (Figure 2, right).[17c,21] All chloro complexes (**2a**−**2g**) exhibit a weak transition around 500 nm which borders a well-defined spectral feature ($\lambda \approx 390$ nm) most intense for **2g**. Past this feature, higher absorptivity is observed in a region crowded with indistinct transitions. This region is not altered by ppy decoration but does change upon extension of tpy's π system

Figure 9. (A) Calculated (blue) and experimental (green) UV−vis absorption spectra for **2a**. The region from 400 to 580 nm is enlarged in the inset to show that the weakest low energy transition is predicted by the calculations. (B) Calculated (blue) and experimental (pink) UV−vis absorption spectra for **3a**. Calculated spectra were generated from Gaussian TD-DFT calculations using Gaussum software with fwhm = 4000 cm^{-1}. Calculated oscillator strengths are included as vertical lines.

(Figures S6 and S7 in the Supporting Information). Higher energies are marked by a strong peak ($\lambda = 234$ nm, $\varepsilon = 56,000-38,000$ M^{-1} cm^{-1}) which remains fairly constant for all chloro compounds (**2a−2g**). Upon substituting cyanide for chloride, this high energy absorption blue-shifts slightly and loses definition while the region of dense transitions becomes more defined showing two distinct features ($\lambda \approx 280$ and 320 nm). Notably, the spectra for cyano materials lack the low energy features near 390 and 500 nm which are prevalent in all of the chloro complexes.

In order to elucidate the character of observed electronic transitions, TD-DFT calculations were performed. For the parent chloro compound (**2a**), the calculations model the low energy region of the spectrum accurately and assign the weakest feature appearing near 500 nm as a mixed MLCT/ILCT transition from the HOMO to the LUMO. Based on its low intensity, this transition has been assigned as a spin forbidden excitation to ^{3}MLCT for similar compounds.[21,24] This assignment may apply here as well but cannot be predicted by TD-DFT. The stronger band near 390 nm is characterized as mixed MLCT/ILCT (HOMO → LUMO + 1 and HOMO − 1 → LUMO). At higher energies between 240 and 330 nm, the calculated spectrum does not accurately depict the crowd of transitions (Figure 9). However, it shows three signals with high oscillator strengths ($\lambda = 285, 295, 324$ nm) which suggest that mixed MLCT/ILCT excitations such as HOMO − 4 → LUMO + 3 appear throughout the region and dominate its lower energies near 324 nm. Meanwhile, mixed MLCT/tpy-centered transitions (HOMO − 6 → LUMO + 1) also contribute near 295 nm, and the highest energy end of the region includes transitions from chloride and ppy π orbitals to ppy π^* orbitals (HOMO − 4 → LUMO + 2). Participation of tpy-centered transitions is consistent with changes observed in the crowded region upon extension of the tpy π system. At higher energies near 234 nm, the experimental absorbance is well represented in the calculations which show that it consists of some ILCT transitions from ppy to tpy but predominately involves transitions from chloride p orbitals and ppy π orbitals to ppy π^* orbitals. Existence of similar ppy and chloride orbitals throughout the chloro series thus explains the consistency of the 234 nm band. The TD-DFT assignments largely agree with those made in other [Ir(N^N^N)(C^N)L]$^+$ materials,[21,24] and they reveal a strong resemblance between the lowest excited states in the new compounds and excitations in [Ir-(ppy)$_2$(bpy)]$^+$ type complexes.[45]

Despite differences in the experimental spectra for **2a** and **3a**, TD-DFT calculations for **3a** show that its transitions mirror the nature of their **2a** analogues. The first excitation of **3a** is not a pure HOMO−LUMO transition as in **2a**, but it maintains

MLCT/ILCT character promoting from the HOMO and nearly identical HOMO − 1 to the tpy-based LUMO. Moreover, although the spectrum of **3a** appears to be missing the prominent low-energy MLCT/ILCT band occurring at 389 nm in **2a**, such a transition is calculated for **3a**. It simply is blue-shifted to ∼370 nm and blends more with the region of dense higher energy transitions. In **3a**, that region still involves a mixture of MLCT/ILCT and ligand-centered transitions, but tpy-centered transitions are less prevalent. Instead, they are blue-shifted contributing more to the band at 225 nm which causes it to differ slightly from the band at 235 nm for **2a**. The significant blue-shifting of transitions, especially prominent low energy MLCT/ILCT transitions, once again reflects the stabilization of occupied frontier orbitals by strong field cyanide.

Emission Spectroscopy. All of the investigated iridium-(III) complexes strongly phosphoresce in acetonitrile in colors ranging from light orange to a greenish blue (Figure 10). The
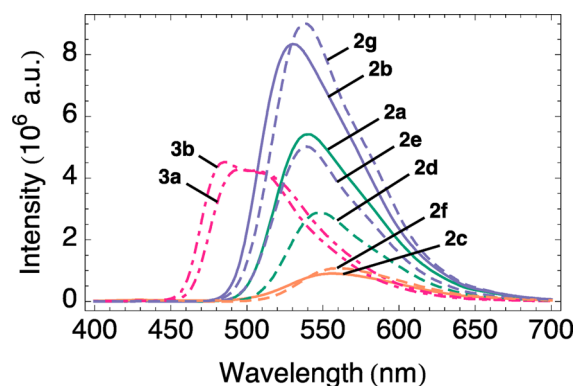

Figure 10. Room temperature emission spectra measured in 10 μM acetonitrile solutions following excitation at 380 nm.

broad and featureless emission bands are consistent with charge transfer and are blue-shifted in comparison to emission from analogous [Ir(ppy)$_2$(bpy)]$^+$ complexes.[8c] In those analogues, the HOMO largely consists of metal orbitals which are significantly destabilized relative to ligand orbitals due to strong σ donation from two cyclometalating carbons. However, as evidenced by the higher metal oxidation potentials in **2a−3b**, their iridium orbitals are less destabilized, which allows for a lower-lying HOMO with more equal anionic ligand and metal contributions. This overrides the slight LUMO stabilization suggested by reduction potentials to produce the blue-shift. The increased ligand-based character of the HOMO also causes

the k_r rate constants of **2a–3b** to be low relative to the rate in $[Ir(ppy)_2(bpy)]^+$ ($k_r = 1.89 \times 10^5$ s^{-1}).[8c]

Within the tpy and phtpy subsets of the chloro series, ppy substituents predictably alter the emission maxima: Blue-shifts accompany HOMO stabilization by fluorine, and red-shifts highlight the opposite effect caused by methoxy. Meanwhile, replacement of the tridentate ligand tpy with phtpy produces only a slight red-shift. Quantum yields decrease with the HOMO–LUMO gap, and emission lifetimes of the chloro compounds correlate reasonably with the HOMO–LUMO gap in accordance with the energy gap law (Figure 11). "Push–pull"
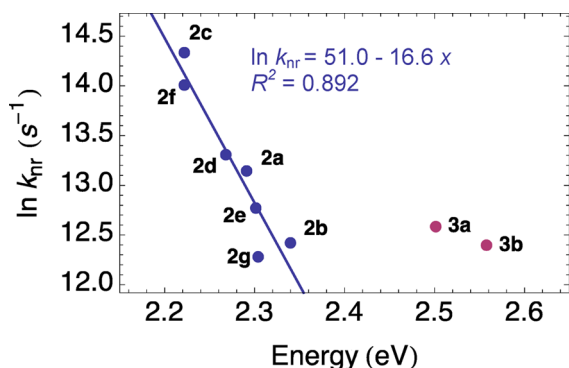

Figure 11. Application of the energy gap law. A linear correlation (blue) is identified to show that all chloro compounds obey the law for a single excited state while the cyano compounds deviate from the trend.

compound **2g** has a relatively long lifetime and strays slightly from the energy gap correlation, which may be an effect of differences in its HOMO detected electrochemically and computationally. Cyano compounds clearly have higher k_{nr} values than predicted from their emission energies by the energy gap law correlation of the chloro compounds in Figure 11. This may occur because the metal–cyanide bond oscillates at a higher frequency ($\tilde{v} \approx 507$ cm^{-1} in $[Ir(CN)_6]^{3-}$)[56] than the weaker metal–chloride bond ($\tilde{v} \approx 293$–302 cm^{-1} in $[IrCl_6]^{3-}$)[57] resulting in more broadly spaced ground state vibrational levels and better overlap of those levels with the excited state. Such overlap can bolster vibrational deactivation pathways insignificant in the chloro series. Deactivation through ^{3}MC states may also become possible since metal–cyanide backbonding stabilizes metal orbitals as evidenced by HOMO stabilization and subsequent blue-shifting of emission in **3a** and **3b**. Table 4 displays all emission lifetimes and radiative decay rates. Lifetimes are longest in **2g** and **3b** and are

impressive in general when compared to similar iridium materials.[8c,17c,46]

Earlier studies highlight the aptitude of DFT calculation protocols for modeling emission maxima in cyclometalated iridium(III) complexes.[8c,17a,58] Similar methodologies were tested here for the new family of luminophores, and results are fully detailed in the Supporting Information (Figures S9 and S10). The most involved approach utilizes the difference in the SCF energy of the triplet excited and singlet ground states at the optimized triplet geometry.[8c,58a] These calculated energies only correlate with luminescence maxima within subsets of very similar complexes while the overall correlation coefficient ($R^2 = 0.66$) is unsatisfactory. Surprisingly, a less common approach taking the total energy difference between singlet ground and triplet excited states at their respective optimized geometries[58] offers the best model for emission energies across the entire family ($R^2 = 0.89$, Figure 12).
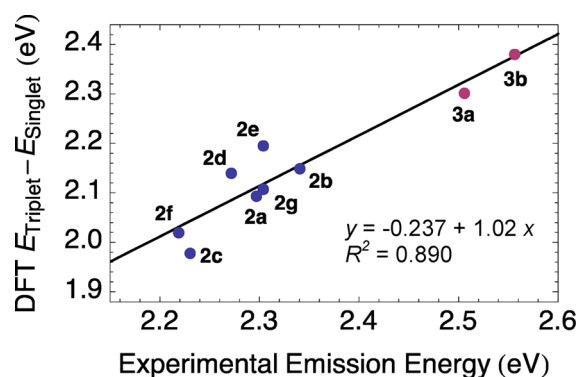

Figure 12. Correlation between experimental emission energy and a computational predictor of emission: the difference in the total energies for T_1 and S_0 calculated at their respective optimized geometries.

Photocatalytic Hydrogen Evolution. In order to demonstrate the photostability of the new luminophores, they were used as photosensitizers for photocatalytic water reduction in acetonitrile solvent with TEA as a sacrificial reductant and K_2PtCl_4 as a catalyst precursor. Figure 13 depicts the H_2 evolution traces for the complexes and the corresponding photosensitizer turnover numbers (TON). Control reactions are shown to produce negligible H_2 indicating that the photosensitizer, catalyst, and light are all essential for water reduction. Differences in the photoreaction conditions employed here and heavily optimized conditions

Table 4. Photophysical Properties

| complex | absorption λ_{max} /nm (intensity/10^4 M^{-1} cm^{-1}) | emission | | | | |
		λ_{max}/ nm	τ/μs	Φ/%	k_{nr}/10^5 s^{-1}	k_r/10^5 s^{-1}
2a	234 (5.61), 270 (3.38), 279sh (3.16), 301 (2.45), 328 (1.70), 389sh (0.52), 499sh (0.11)	541	1.674	15.0	5.07	0.90
2b	237 (5.11), 270 (3.46), 280sh (3.06), 300 (2.39), 327 (1.89), 388sh (0.40), 495sh (0.09)	530	2.849	28.6	2.51	1.00
2c	234 (4.24), 254 (3.32), 280 (3.22), 307 (2.62), 327 (2.07), 359sh (0.94), 494sh (0.11)	558	0.580	3.2	16.70	0.54
2d	238 (3.80), 275 (3.73), 283 (3.75), 300 (3.04), 330sh (1.50), 369 (0.71), 398 (0.66), 505sh (0.16)	547	1.433	13.2	6.06	0.92
2e	238 (4.37), 275 (4.30), 284 (4.12), 301 (3.45), 327sh (1.89), 360 (0.76), 393 (0.61), 501 (0.07)	539	2.149	24.7	3.51	1.15
2f	233 (4.46), 284 (4.76), 306sh (3.64), 329sh (2.26), 362 (1.25), 398sh (0.80), 507sh (0.30)	558	0.789	4.6	12.09	0.58
2g	235 (4.43), 274 (4.12), 282 (4.04), 324sh (1.97), 370 (1.15), 396 (1.15), 493sh (0.11)	538	3.486	25.2	2.14	0.73
3a	225sh (3.86), 272 (3.42), 280 (3.33), 320 (1.82), 368sh (0.49)	496	2.874	15.5	2.94	0.54
3b	226 (3.86), 271 (3.85), 280 (3.65), 319 (2.13), 367sh (0.37)	485	3.118	24.5	2.42	0.78
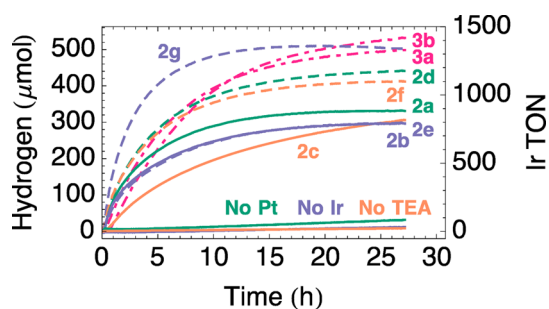
Figure 13. Performance of complexes **2a**–**3b** as photosensitizers for photocatalytic hydrogen evolution. Reactions were performed in 9 mL of 8:1 ACN/H_2O with 0.075 mM photosensitizer, 300 nmol of K_2PtCl_4, and 1 mL of TEA sacrificial reductant. The amount of hydrogen evolved is noted along with the number of turnovers of the iridium photosensitizer. Control runs are indicated.

Figure 14. Stern−Volmer plots showing emission quenching as a function of oxygen partial pressure for **2b** (purple) and **3b** (pink) in acetonitrile.

used in previous studies complicate direct comparison. Still, the photosensitizer turnover numbers achieved by the new luminophores are generally less than those obtained with members of the prevalent $[Ir(ppy)_2(bpy)]^+$ family in less coordinating THF with palladium or rhodium catalyst.[13d,59] In acetonitrile, though, those well-known photosensitizers decompose via displacement of their bpy ligands (Ir TON < 325 with Pd catalyst, Ir TON < 100 with Pt catalyst) failing to match the strong performance observed for the new materials in the highly coordinating solvent.[59,60] Thus, the use of a tridentate ligand instead of bipyridine seems to impart robustness to **2a**–**3b**.

In the new family, the cyanide-containing complexes (**3a** and **3b**) generate more H_2 than chloro complexes with **3b** achieving up to 1440 turnovers. These compounds likely outlast their chloro analogues because they decompose less readily through monodentate ligand dissociation as suggested by the full reversibility of their reduction processes. Meanwhile, **2g** is a standout among chloro complexes giving fast initial reaction rates and 1300 turnovers. The three best photosensitizers (**2g**, **3a**, **3b**) have the longest excited state lifetimes, which improve performance by expanding the time frame for transfer of excited electrons to the catalyst. Performance of **2g** may also be strengthened by its "push−pull" design or unique HOMO character.

Oxygen Quenching. Photosensitizers which are sensitive to paramagnetic quenching by O_2 cannot be envisioned for oxygen-generating systems such as complete water splitting. In order to evaluate susceptibility of the new complexes to this common photosensitizer weakness, Stern−Volmer analysis was completed for two complexes with long-lived excited states, **2b** and **3b**. Emission was measured under different percentages of oxygen in acetonitrile. The measured slopes of the Stern−Volmer plots shown in Figure 14 indicate that the excited states of both **2b** ($K_{svP} = 0.00634$ mbar^{-1}, $k_q = 2.49 \times 10^8$ M^{-1} s^{-1}) and **3b** ($K_{svP} = 0.00807$ mbar^{-1}, $k_q = 2.90 \times 10^8$ M^{-1} s^{-1}) are more resistant to oxygen quenching than the excited states of many other luminophores.[9a,61] For comparison, in acetonitrile, the K_{svP} values for the archetypical dye $[Ru(bpy)_3]^{2+}$ and the iridium(III) photosensitizer $[Ir(ppy)_2(bpy)]^+$ are 0.024 mbar^{-1} ($k_q = 2.9 \times 10^9$ M^{-1} s^{-1}) and 0.026 mbar^{-1} ($k_q = 8.8 \times 10^9$ M^{-1} s^{-1}) respectively.[9a]
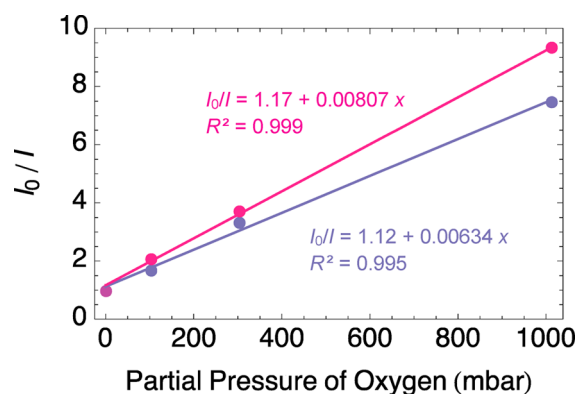
■ CONCLUSION

A family of luminophores has been prepared to further explore the structure $[Ir(tpy)(ppy)Cl]^+$ presented previously as a catalyst for CO_2 reduction. The new luminophores were readily synthesized as a single isomer which orients ppy's cyclometalating carbon trans to the monodentate ligand. Adding aryl groups to the tpy ligand fails to tune the LUMO located there. However, the HOMO composed of monodentate ligand, metal, and ppy orbitals is significantly stabilized by increases in the electron deficiency of the ppy and the field strength of the monodentate ligand. Choice of monodentate ligand also affects stability during redox processes: Both chloride and cyanide appear to dissociate upon oxidation and electrospray ionization, but only chloride leads to instability during reduction. The HOMO of the investigated luminophores is more ligand-based and stabilized than the HOMO of popular $[Ir(ppy)_2(bpy)]^+$ photosensitizers producing a blue-shifted emission. Lifetimes and quantum yields of emission are impressive, especially in cyano complexes and the specially designed push−pull derivative. Those compounds are also leaders in photosensitization of photocatalytic hydrogen evolution. Meanwhile, all of the compounds show enhanced photostability by turning over more than other iridium photosensitizers in harsh coordinating solvent. In the future, compounds with the explored $[Ir(tpy)(ppy)Cl]^+$ motif may be considered as photosensitizers for complete water splitting based on their photostability as well as the relatively high tolerance of their excited state for oxygen.

■ ASSOCIATED CONTENT

Ⓢ Supporting Information

All NMR and UV−vis absorption spectra along with selected mass spectra and DFT results. Additional electrochemical measurements including a scan rate dependence illustration. Detailed crystallographic parameters and X-ray crystallographic data for **2c** in CIF format. This material is available free of charge via the Internet at http://pubs.acs.org.

■ AUTHOR INFORMATION

Corresponding Author

*E-mail: bern@cmu.edu.

Notes

The authors declare no competing financial interest.

■ REFERENCES

(1) Juris, A.; Balzani, V.; Berigelletti, F.; Campagna, S.; Belser, P.; von Zelewsky, A. *Coord. Chem. Rev.* **1988**, *84*, 85−277.

(2) Durham, B.; Caspar, J. V.; Nagle, J. K.; Meyer, T. J. *J. Am. Chem. Soc.* **1982**, *104*, 4803−4810.

(3) Van Houten, J.; Watts, R. J. *J. Am. Chem. Soc.* **1976**, *98* (16), 4853−4858.

(4) Williams, J. A. G. *Top. Curr. Chem.* **2007**, *281*, 205−268.

(5) Armaroli, N.; Accorsi, G.; Cardinali, F.; Listorti, A. *Top. Curr. Chem.* **2007**, *280*, 69−115.

(6) Kirgan, R. A.; Sullivan, B. P.; Rillema, D. P. *Top. Curr. Chem.* **2007**, *281*, 45−100.

(7) Kumaresan, D.; Shankar, K.; Vaidya, S.; Schmehl, R. H. *Top. Curr. Chem.* **2007**, *281*, 101−142.

(8) (a) Lowry, M. S.; Bernhard, S. *Chem.—Eur. J.* **2006**, *12*, 7970−7977. (b) Ulbricht, C.; Beyer, B.; Friebe, C.; Winter, A.; Schubert, U. S. *Adv. Mater.* **2009**, *21*, 4418−4441. (c) Lowry, M. S.; Hudson, W. R.; Pascal, R. A., Jr.; Bernhard, S. *J. Am. Chem. Soc.* **2004**, *126*, 14129−14135.

(9) (a) Jenkins, D. M.; Bernhard, S. *Inorg. Chem.* **2010**, *49*, 11297−11308. (b) Gianini, M.; Forster, A.; Haag, P.; von Zelewsky, A.; Stoeckli-Evans, H. *Inorg. Chem.* **1996**, *35*, 4889−4895.

(10) Wenger, O. S. *Coord. Chem. Rev.* **2009**, *253*, 1439−1457.

(11) Lo, K. K. W.; Zhang, K. Y.; Leung, S. K.; Tang, M. C. *Angew. Chem., Int. Ed.* **2008**, *47*, 2213−2216.

(12) (a) Rausch, A. F.; Thompson, M. E.; Yersin, H. *J. Phys. Chem. A* **2009**, *113*, 5927−5932. (b) Slinker, J. D.; Rivnay, J.; Moskowitz, J. S.; Parker, J. B.; Bernhard, S.; Abruña, H. D.; Malliaras, G. G. *J. Mater. Chem.* **2007**, *17*, 2976−2988.

(13) (a) Gärtner, F.; Sundararaju, B.; Surkus, A. E.; Boddien, A.; Loges, B.; Junge, H.; Dixneuf, P. H.; Beller, M. *Angew. Chem., Int. Ed.* **2009**, *48*, 9962−9965. (b) Wang, C.; deKrafft, K. E.; Lin, W. B. *J. Am. Chem. Soc.* **2012**, *134*, 7211−7214. (c) Metz, S.; Bernhard, S. *Chem. Commun.* **2010**, *46*, 7551−7553. (d) Cline, E. D.; Adamson, S. E.; Bernhard, S. *Inorg. Chem.* **2008**, *47*, 10378−10388. (e) DiSalle, B. F.; Bernhard, S. *J. Am. Chem. Soc.* **2011**, *133*, 11819−11821.

(14) (a) Condie, A. G.; Gonzalez-Gomez, J. C.; Stephenson, C. R. J. *J. Am. Chem. Soc.* **2010**, *132*, 1464−1465. (b) Lalevée, J.; Peter, M.; Dumur, F.; Gigmes, D.; Blanchard, N.; Tehfe, M. A.; Morlet-Savary, F.; Fouassier, J. P. *Chem.—Eur. J.* **2011**, *17*, 15027−15031. (c) Rueping, M.; Zhu, S. Q.; Koenigs, R. M. *Chem. Commun.* **2011**, *47*, 8679−8681. (d) Nagib, D. A.; Scott, M. E.; MacMillan, D. W. C. *J. Am. Chem. Soc.* **2009**, *131*, 10875−10877.

(15) (a) Flynn, C. M., Jr.; Demas, J. N. *J. Am. Chem. Soc.* **1974**, *96* (6), 1959−1960. (b) Demas, J. N.; Harris, E. W.; Flynn, C. M., Jr.; Diemente, D. *J. Am. Chem. Soc.* **1975**, *97* (13), 3838−3839.

(16) (a) Ayala, N. P.; Flynn, C. M.; Sacksteder, L.; Demas, J. N.; DeGraff, B. A. *J. Am. Chem. Soc.* **1990**, *112*, 3837−3844. (b) Collin, J.-P.; Dixon, I. M.; Sauvage, J.-P.; Williams, J. A. G.; Barigelletti, F.; Flamigni, L. *J. Am. Chem. Soc.* **1999**, *121*, 5009−5016.

(17) (a) Tamayo, A. B.; Alleyne, B. D.; Djurovich, P. I.; Lamansky, S.; Tsyba, I.; Ho, N. N.; Bau, R.; Thompson, M. E. *J. Am. Chem. Soc.* **2003**, *125*, 7377−7387. (b) Tsuboyama, A.; Iwawaki, H.; Furugori, M.; Mukaide, T.; Kamatani, J.; Igawa, S.; Moriyama, T.; Miura, S.; Takiguchi, T.; Okada, S.; Hoshino, M.; Ueno, K. *J. Am. Chem. Soc.* **2003**, *125*, 12971−12979. (c) Baranoff, E.; Yum, J.-H.; Graetzel, M.; Nazeeruddin, Md. K. *J. Organomet. Chem.* **2009**, *694*, 2661−2670.

(18) Tinker, L. L.; Bernhard, S. *Inorg. Chem.* **2009**, *48* (22), 10507−10511.

(19) (a) Polson, M.; Fracasso, S.; Bertolasi, V.; Ravaglia, M.; Scandola, F. *Inorg. Chem.* **2004**, *43* (6), 1950−1956. (b) Polson, M.; Ravaglia, M.; Fracasso, S.; Garavelli, M.; Scandola, F. *Inorg. Chem.* **2005**, *44*, 1282−1289.

(20) Whittle, V. L.; Williams, J. A. G. *Inorg. Chem.* **2008**, *47*, 6596−6607.

(21) Bexon, A. J. S.; Williams, J. A. G. *C. R. Chim.* **2005**, *8*, 1326−1335.

(22) Williams, J. A. G.; Wilkinson, A. J.; Whittle, V. L. *Dalton Trans.* **2008**, 6513−6515.

(23) (a) Yoshikawa, N.; Matsumura-Inoue, T. *Anal. Sci.* **2003**, *19*, 761−765. (b) Yoshikawa, N.; Yamabe, S.; Kanehisa, N.; Kai, Y.; Takashima, H.; Tsukahara, K. *Eur. J. Inorg. Chem.* **2007**, 1911−1919.

(24) Obara, S.; Itabashi, M.; Okuda, F.; Tamaki, S.; Tanabe, Y.; Ishii, Y.; Nozaki, K.; Haga, M. *Inorg. Chem.* **2006**, *45*, 8907−8921.

(25) Sato, S.; Morikawam, T.; Kajino, T.; Ishitani, O. *Angew. Chem., Int. Ed.* **2013**, *52*, 988−992.

(26) Wang, J.; Hanan, G. S. *Synlett* **2005**, *No. 8*, 1251−1254.

(27) Song, C.; Ye, Z.; Wang, G.; Yuan, J.; Guan, Y. *Chem.—Eur. J.* **2010**, *16* (22), 6464−6472.

(28) Constable, E. C.; Lewis, J.; Liptrot, M. C.; Raithby, P. R. *Inorg. Chim. Acta* **1990**, *178*, 47−54.

(29) Spek, A. L. *J. Appl. Crystallogr.* **2003**, *36*, 7−13.

(30) Sheldrick, G. M. *SADABS Version 2.03*; University of Göttingen: Göttingen, Germany, 2002.

(31) Sheldrick, G. M. *SHELXTL 6.1, Crystallographic Computing System*; Bruker Analytical X-Ray System: Madison, WI, 2000.

(32) Zysman-Colman, E.; Slinker, J.; Parker, J.; Malliaras, G.; Bernhard, S. *Chem. Mater.* **2008**, *20*, 388−396.

(33) Connelly, N. G.; Geiger, W. E. *Chem. Rev.* **1996**, *96*, 877−910.

(34) Frisch, M. J.; Trucks, G. W.; Schlegel, H. B.; Scuseria, G. E.; Robb, M. A.; Cheeseman, J. R.; Montgomery, Jr., J. A.; Vreven, T.; Kudin, K. N.; Burant, J. C.; Millam, J. M.; Iyengar, S. S.; Tomasi, J.; Barone, V.; Mennucci, B.; Cossi, M.; Scalmani, G.; Rega, N.; Petersson, G. A.; Nakatsuji, H.; Hada, M.; Ehara, M.; Toyota, K.; Fukuda, R.; Hasegawa, J.; Ishida, M.; Nakajima, T.; Honda, Y.; Kitao, O.; Nakai, H.; Klene, M.; Li, X.; Knox, J. E.; Hratchian, H. P.; Cross, J. B.; Bakken, V.; Adamo, C.; Jaramillo, J.; Gomperts, R.; Stratmann, R. E.; Yazyev, O.; Austin, A. J.; Cammi, R.; Pomelli, C.; Ochterski, J. W.; Ayala, P. Y.; Morokuma, K.; Voth, G. A.; Salvador, P.; Dannenberg, J. J.; Zakrzewski, V. G.; Dapprich, S.; Daniels, A. D.; Strain, M. C.; Farkas, O.; Malick, D. K.; Rabuck, A. D.; Raghavachari, K.; Foresman, J. B.; Ortiz, J. V.; Cui, Q.; Baboul, A. G.; Clifford, S.; Cioslowski, J.; Stefanov, B. B.; Liu, G.; Liashenko, A.; Piskorz, P.; Komaromi, I.; Martin, R. L.; Fox, D. J.; Keith, T.; Al-Laham, M. A.; Peng, C. Y.; Nanayakkara, A.; Challacombe, M.; Gill, P. M. W.; Johnson, B.; Chen, W.; Wong, M. W.; Gonzalez, C.; Pople, J. A. *Gaussian 03, revision C.02*; Gaussian Inc.: Wallingford, CT, 2004.

(35) Becke, A. D. *J. Chem. Phys.* **1993**, *98*, 5648−5652.

(36) Lee, C.; Yang, W.; Parr, R. G. *Phys. Rev. B: Condens. Matter Mater. Phys.* **1988**, *37*, 785−789.

(37) Miehlich, B.; Savin, A.; Stoll, H.; Preuss, H. *Chem. Phys. Lett.* **1989**, *157*, 200−206.

(38) (a) Hay, P. J.; Wadt, W. R. *J. Chem. Phys.* **1985**, *82*, 299−310. (b) Hay, P. J.; Wadt, W. R. *J. Chem. Phys.* **1985**, *82*, 270−283. (c) Wadt, W. R.; Hay, P. J. *J. Chem. Phys.* **1985**, *82*, 284−298.

(39) (a) O'Boyle, N. M. *GaussSum 2.0*; Dublin City University: Dublin, Ireland, 2006. Available at http://gaussum.sourceforge.net/. (b) O'Boyle, N. M.; Tenderholt, A. L.; Langner, K. M. *J. Comput. Chem.* **2008**, *29*, 839−845.

(40) Abergel, R. J.; D'Aleo, A.; Leung, C. N. P.; Shuh, D. K.; Raymond, K. N. *Inorg. Chem.* **2009**, *48*, 10868−10870.

(41) Caspar, J. V.; Meyer, T. J. *J. Am. Chem. Soc.* **1983**, *105*, 5583−5590.

(42) Montalti, M.; Credi, A.; Prodi, L.; Gandolfi, M. T. *Handbook of Photochemistry*, 3rd ed.; CRC Press: Boca Raton, 2006.

(43) Morris, K. J.; Roach, M. S.; Xu, W.; Demas, J. N.; DeGraff, B. A. *Anal. Chem.* **2007**, *79*, 9310−9314.

(44) Lowry, M. S.; Goldsmith, J. I.; Slinker, J. D.; Rohl, R.; Pascal, R. A., Jr.; Malliaras, G. G.; Bernhard, S. *Chem. Mater.* **2005**, *17*, 5712−5719.

(45) Chirdon, D. N.; McCusker, C. E.; Castellano, F. N.; Bernhard, S. *Inorg. Chem.* **2013**, *52*, 8795−8804.

(46) Goldsmith, J. I.; Hudson, W. R.; Lowry, M. S.; Anderson, T. H.; Bernhard, S. *J. Am. Chem. Soc.* **2005**, *127*, 7502−7510.

(47) Flamigni, L.; Barbieri, A.; Sabatini, C.; Ventura, B.; Barigelletti, F. *Top. Curr. Chem.* **2007**, *281*, 143−203.

(48) Yoshikawa, N.; Yamabe, S.; Kanehisa, N.; Kai, Y.; Takashima, H.; Tsukahara, K. *Inorg. Chim. Acta* **2009**, *362* (2), 361−371.

(49) Yoshikawa, N.; Sakamoto, J.; Kanehisa, N.; Kai, Y.; Matsumura-Inoue, T.; Takashima, H.; Tsukahara, K. *Acta Crystallogr., Sect. E: Struct. Rep. Online* **2003**, *59* (10), 830−382.

(50) Breu, J.; Stossel, P.; Schrader, S.; Starukhin, A.; Finkenzeller, W. J.; Yersin, H. *Chem. Mater.* **2005**, *17* (7), 1745−1752.

(51) Yutaka, T.; Obara, S.; Haga, M.; Yokoyama, Y.; Sakai, K. *Acta Crystallogr., Sect. E: Struct. Rep. Online* **2005**, *61* (7), m1357−m1359.

(52) Varetto, U. *Molekel: 5.4.0.8*; Swiss National Supercomputing Centre: Lugano, Switzerland.

(53) Breikss, A. I.; Abruña, H. D. *J. Electroanal. Chem.* **1986**, *201*, 347−358.

(54) Hawecker, J.; Lehn, J. M.; Ziessel, R. *J. Chem. Soc., Chem. Commun.* **1983**, 536−538.

(55) Kalyanasundaram, K. *Photochemistry of Polypyridine and Porphyrin Complexes*; Academic Press: San Diego, CA, 1992.

(56) Swanson, B. I.; Jones, L. H. *Inorg. Chem.* **1974**, *13* (2), 313−316.

(57) Herbelin, F.; Herbelin, J. D.; Mathieu, J. P.; Poulet, H. *Spectrochim. Acta* **1966**, *22*, 1515−1522.

(58) (a) Donato, L.; Abel, P.; Zysman-Colman, E. *Dalton Trans.* **2013**, *42*, 8402−8412. (b) Ladouceur, S.; Fortin, D.; Zysman-Colman, E. *Inorg. Chem.* **2011**, *50*, 11514−11526.

(59) Curtin, P. N.; Tinker, L. L.; Burgess, C. M.; Cline, E. D.; Bernhard, S. *Inorg. Chem.* **2009**, *48*, 10498−10506.

(60) Tinker, L. L.; McDaniel, N. D.; Curtin, P. N.; Smith, C. K.; Ireland, M. J.; Bernhard, S. *Chem.—Eur. J.* **2007**, *13* (31), 8726−8732.

(61) Demas, J. N.; Harris, E. W.; McBride, R. P. *J. Am. Chem. Soc.* **1977**, *99* (11), 3547−3551.